Electronic Supplementary Material (ESI) for Catalysis Science & Technology.

Supporting Information

Layer-dependent Catalysis of MoS_2/Graphene Nanoribbon Composites for Efficient Hydrodesulfurization

Lan Yang[a], *Xuzhen Wang*[a,b,*], *Yang Liu*[b], *Zhengfa Yu*[b] , *Rui Li*[a], *Jieshan Qiu*[b]

[a] State Key Laboratory of Fine Chemicals and School of Chemistry, Dalian University of Technology, Dalian, China. [b] Liaoning Key Lab for Energy Materials and Chemical Engineering, PSU-DUT Joint Center for Energy Research, Faculty of Chemical, Environmental & Biological Science and Technology, Dalian University of Technology, Dalian, China.

E-mail: xzwang@dlut.edu.cn

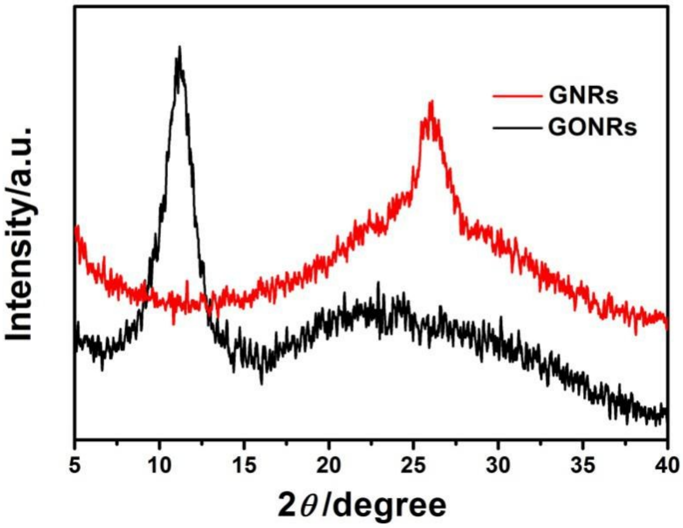

Figure S1 XRD patterns of GNRs and GONRs.

X-ray diffraction pattern of GONRs shows a major peak at 2θ =11° corresponding to an interlayer spacing of 0.8 nm, while GNRs derived from hydrazine reduction of GONRs give rise to a strong peak at 2θ =25.7^{o} which indicates the serious restack of graphene nanoribbons like graphene during the reduction process[1].

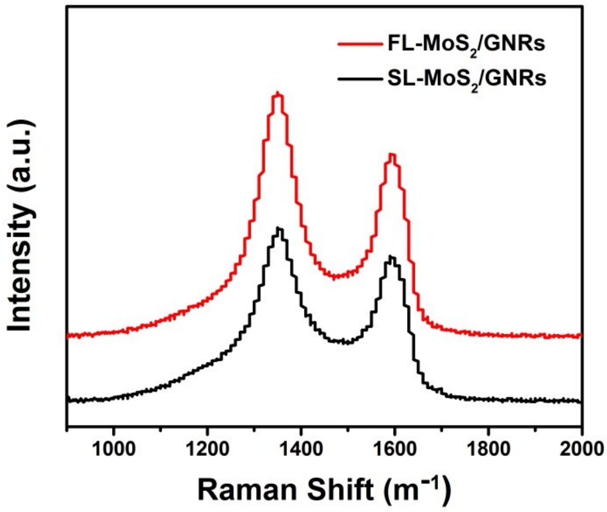

Figure S2 Raman spectra of FL-MoS$_2$/GNRs and SL-MoS$_2$/GNRs.

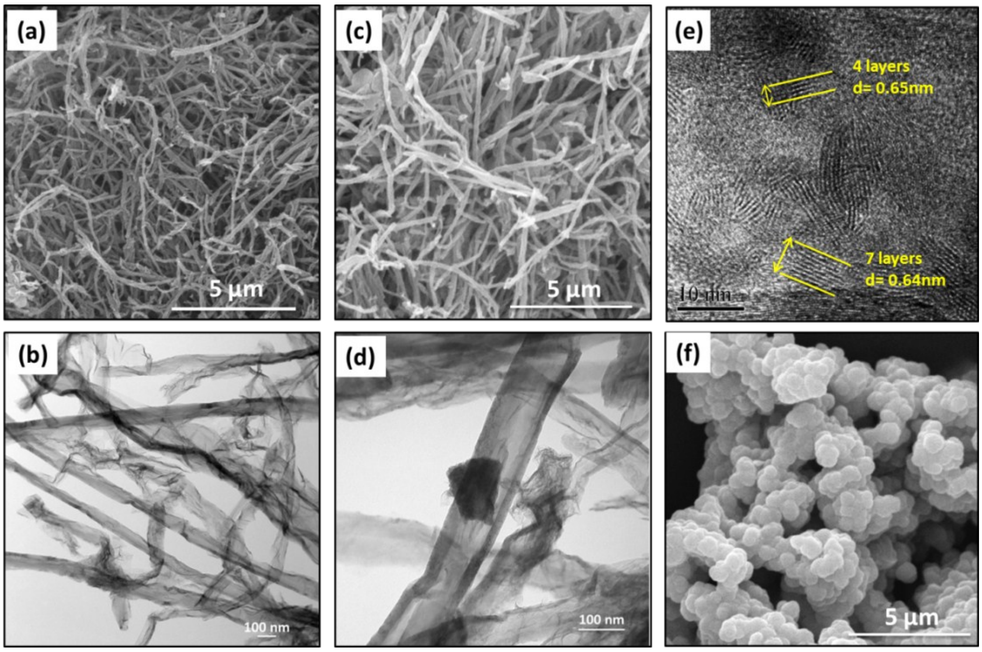

Figure S3. (a) SEM image and (b) TEM image of GNRs. (c) SEM image, (d) TEM image and (e) HR-TEM image of FL-MoS$_2$/GNRs. (f) SEM image of ML-MoS$_2$.

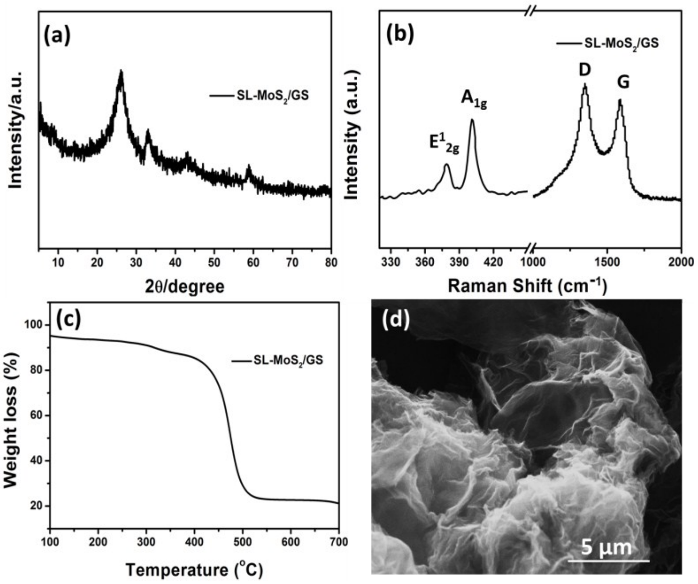

Figure S4 (a) XRD pattern, (b) Raman spectra, (c) TGA curve and (d) SEM image of SL-MoS_2/GS.

Fig. S4a shows the XRD pattern of SL-MoS_2/GS, the absence of (002) reflection (2θ = 14.2°) evidences that only single-layer MoS_2 exist in the SL-MoS_2/GS. As shown in Fig.S4b, two Raman peaks were located at 379 cm^{-1} (E^1_{2g}) and 401 cm^{-1} (A_{1g}) with Δk = 22 cm^{-1}. The calculated value of I_D/I_G for SL-MoS_2/GS is 1.16. The content of Mo calculated from TGA in SL-MoS_2/GS is 14.2 wt%.

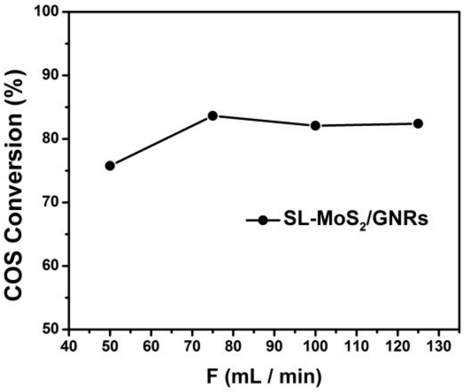

Figure S5 Effect of external diffusion on conversion of COS.

The changes of COS conversion influenced by different total gas flow which controlled in the same space velocity by filling the different quality of catalyst was shown. The specific value of total gas flow and quality of catalyst is controlled in 10 (mL/min) /5 (mg) while the concentration of COS is 500 ppm and the volume percentage of H_2 is 10% vol balanced with N_2. As shown in Figure S5, the COS conversion rate was increased with the increasing of the total gas flow. There is no external diffusion effect when the total gas flow is larger than 75 mL/min as a result of the invariability of COS conversion. As for the MoS_2/GNRs hybrids are very thin sheet-like structure, the pathway for the gases diffusion is very short, as a result, the internal diffusion limitation is negligible in this reaction. The apparent reaction order is measured at 100 mL/min in order to guarantee the experimental accuracy.

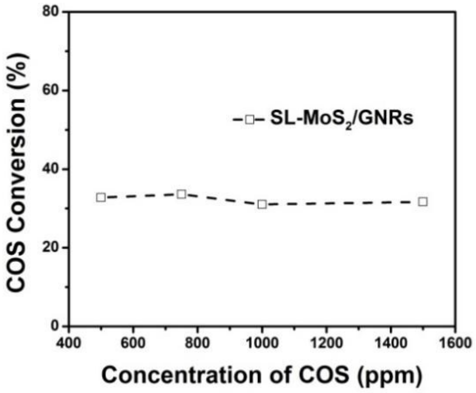

Figure S6 Effect of COS concentration on conversion of COS.

The reaction order in COS is measured by changing the concentration of COS in the case of excessive amount of hydrogen. It is obviously found that the COS conversion does not change with different concentration of COS under different test temperatures. As a result, over SL-MoS_2/GNRs, the reaction rate of COS was zero.

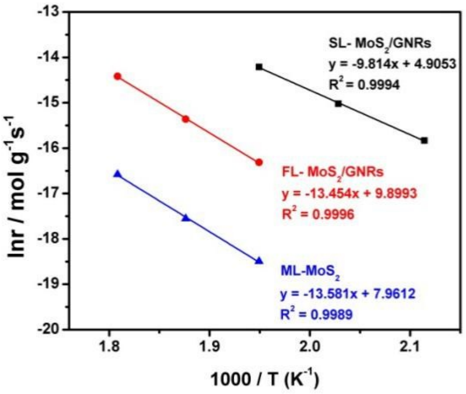

Figure S7 Arrhenius plots of reaction rates for HDS of COS over the catalysts with different layer structure of MoS_2. (Reaction conditions: 500 ppm COS, 10% vol. H_2, balanced with N_2)

Figure S7 shows the Arrhenius plots over three catalysts with different layer structures of MoS_2 at COS conversion in the range of 15-20% (at which the reaction temperature range was 20 ^{o}C). The data of apparent active energies (E_a) was calculated from the slope of the line. It can be arrived at the conclusion that the E_a of ML-MoS_2 catalyst with multi-layer structure of MoS_2 was 112.9 kJ·mol^{-1}, which was higher than 111.9 kJ·mol^{-1} of FL-MoS_2/GNRs and 81.6 kJ·mol^{-1} of SL-MoS_2/GNRs.

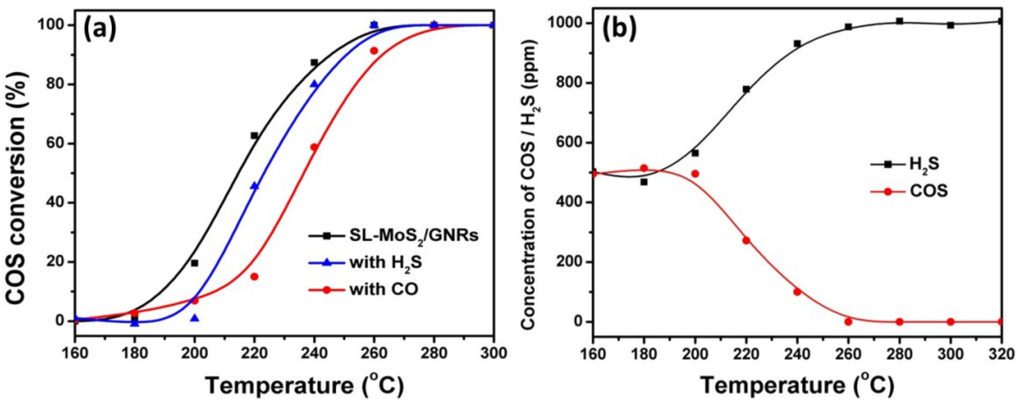

Figure S8 (a) Temperature-dependent conversion of COS over SL-MoS_2/GNRs, for feeding gas 500 ppm of COS/N_2 with 500 ppm H_2S or 800 ppm CO at *GHSV* = 8,000 h^{-1}; (b) Temperature-dependent concentration of COS and H_2S over SL-MoS_2/GNRs for feeding gas 500 ppm of COS/N_2 with 500 ppm H_2S at GHSV=8,000 h^{-1}.

Figure S8a shows the COS conversion results over the SL-MoS_2/GNRs catalyst for the feed gas of 500 ppm COS together with 500ppm H_2S or 800 ppm CO in N_2. The inhibition effects of impurity gases on the reaction over the catalyst were quite limited. Over the catalyst, T_{90} (the temperature for COS conversion reaching 90%) of the reaction in the feeding gas of 500 ppm COS/N_2 was 240 °C. When H_2S (500 ppm) or CO (800 ppm) was introduced into the feed gas, T_{90} was increased to 250 °C and 260 °C, respectively. Temperature-dependent concentration of COS and H_2S over SL-MoS_2/GNRs with feeding gas of COS (500 ppm) and H_2S (500 ppm) balanced with N_2 was shown in Figure S8b. With the increasing of temperature, it can be indicated that the concentration of COS increased, while the concentration of H_2S decreased below 180 °C, which should be attributed to the adverse reaction of hydrogenation:

$$H_2S + CO = COS + H_2 \qquad (S1)$$

In this case, H_2S is extremely easy to transform into COS with the existence of CO. However, with the increasing temperature from 200 to 300 °C, the concentration of COS decreased and the concentration of H_2S increased remarkably due to the favorable hydrogenation at high temperature.

$$COS + H_2 = H_2S + CO \qquad (S2)$$

In a word, it is easy for H_2S to transform into COS at low temperature while adverse reaction will take place at high temperature over SL-MoS_2/GNRs.

Statistical analysis methods of the MoS_2 slabs

The stacking numbers and lengths of the MoS_2 slabs were obtained from statistical analysis based on many HR-TEM images. To make a quantitative comparison, the slab lengths and stacking layers were obtained through statistical analyses based on at least 300 slabs taken from the different parts of each sample. The average number of layers (N_m) and average slab length (L_m) have been calculated according to the first moment of distribution[2, 3]:

$$L_m = \sum_{i=1}^{x} x_i l_i / \sum_{i=1}^{x} x_i \qquad \text{(S3)}$$

$$N_m = \sum_{i=1}^{y} y_i N_i / \sum_{i=1}^{y} y_i \qquad \text{(S4)}$$

Where x_i is the number of slabs with length l_i, and y_i is the number of slabs with N_i layers. In addition, a dispersion indicator of the active surface of the crystal which was denoted as 'f_{Mo}' present the average fraction of Mo atoms on the edge of MoS_2 crystals. The f_{Mo} value is determined from the following equation assuming that the MoS_2 slabs are present as perfect hexagons. The equation is expressed as

$$f_{Mo} = (\sum_{i=1}^{t} 6n_i - 6) / (\sum_{i=1}^{t} 3n_i^2 - 3n_i + 1) \qquad \text{(S5)}$$

Where n_i is the number of Mo atoms along one edge of a MoS_2 slab determined from its length (L=0.32 (n_i-1) nm) and t is the total number of slabs. In the equation, the numerator is the number of atoms in the active surface (edges) and the denominator is the total number of Mo atoms in the crystal[2].

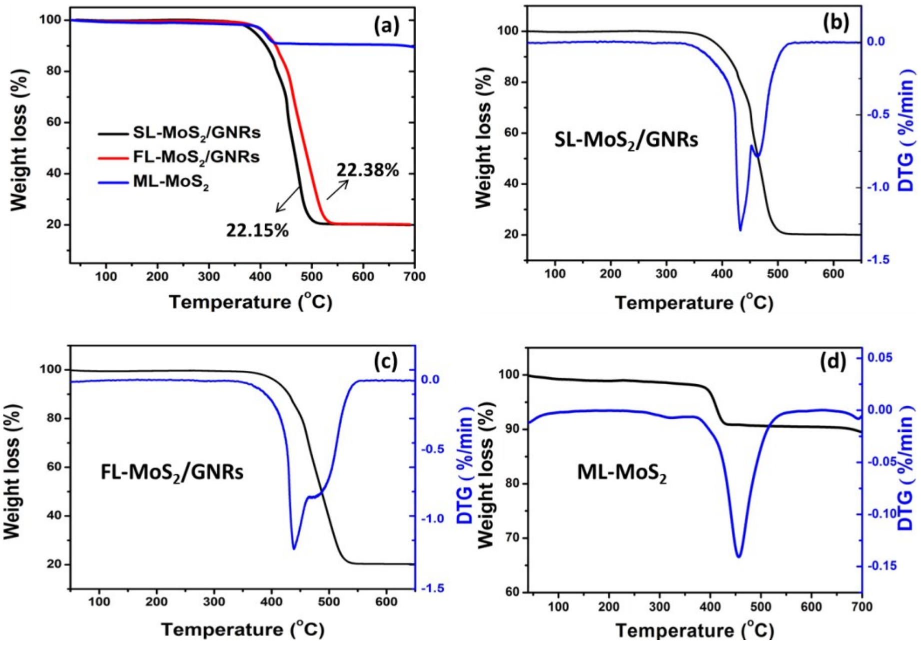

Figure S9. (a) TGA curves of SL-MoS_2/GNRs, FL-MoS_2/GNRs and ML-MoS_2. DTG curves of (b) SL-MoS_2/GNRs, (c) FL-MoS_2/RGO and (d) ML-MoS_2 measured at a heating rate of 10 ^{o}C min^{-1} in a flowing air.

TGA and DTG curves of SL-MoS_2/GNRs, FL-MoS_2/GNRs and ML-MoS_2 measured at a heating rate of 10 ^{o}C min^{-1} in a flowing air were shown in Figure S9a. During the materials preparation, the CTA^+ would insert between MoS_2 layers to restrict their stack and form the single MoS_2 layer structures. After heat treatment, CTA^+ was transformed into amorphous carbon interlaid between monolayer MoS_2 sheets[4]. As shown in Fig. S9b-c, weight loss appears at approximately 360 ^{o}C and finishes at about 550 ^{o}C, which can probably be attributed to the oxidation of amorphous carbon and GNRs, as well as the oxidation reaction of MoS_2. Fig.S9d shows that as a result of the oxidization reaction of MoS_2 to MoO_3, MoS_2 start to lose weight at approximately 420 ^{o}C and overall weight loss is 10.5% which has a well agreement with the theoretical value (10.1%). It has been reported that the carbon were oxidized completely, only MoO_3 remained when treated at 700 ^{o}C in a floating air[5-7]. The content of MoS_2 in SL-MoS_2/GNRs is 22.2%, which is approximately the same to the FL-MoS_2/GNRs (22.4%).

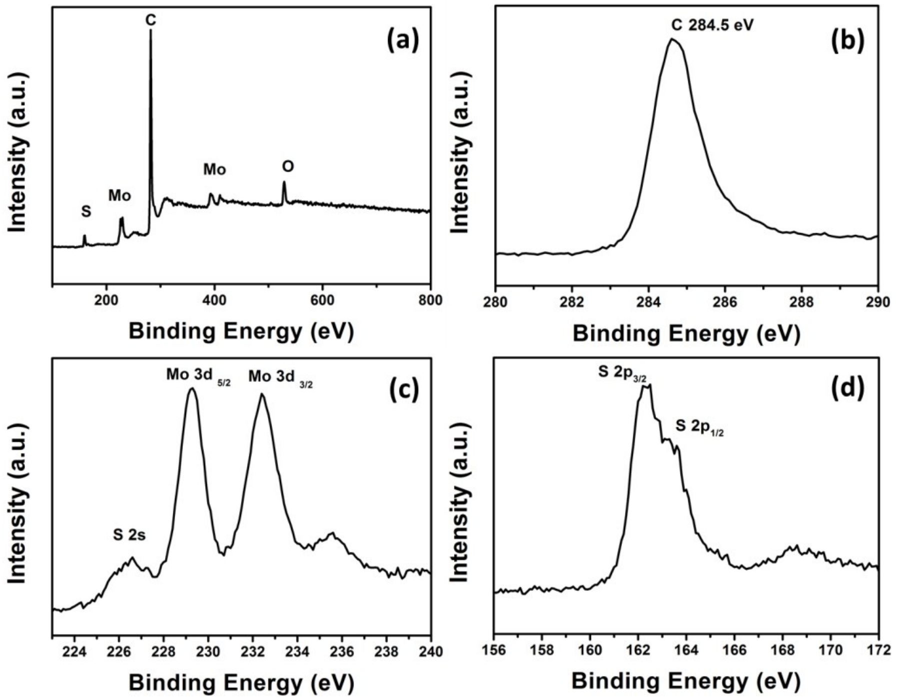

Figure S10 (a) XPS survey spectrum and high-resolution scans for the (b) C 1s, (c) Mo 3d and (d) S 2p electrons of FL-MoS_2/GNRs.

As shown in Figure S10a the elements of C, Mo, S and O can be clearly identified. The C1s characteristic peak at 284.5 eV shown in Figure S10b also coincided with the sp^2 carbon of the graphene (oxide) scaffold. The Mo 3d XPS spectrum of FL-MoS_2/GNRs sample (Figure S9c) shows two broad peaks at 229.2 and 232.4 eV, which can be indexed as the doublet Mo $3d_{5/2}$ and Mo $3d_{3/2}$, respectively. The peak at 235.5 eV is due to the Mo^{+6} ions in MoO_3. A small S 2s peak is located at 226.4 eV. The peaks at 162.1 and 163.4 eV, corresponding to the S $2p_{3/2}$ and S $2p_{/1/2}$ of divalent sulfide ions (S^{2-}), are observed in Figure S10d.

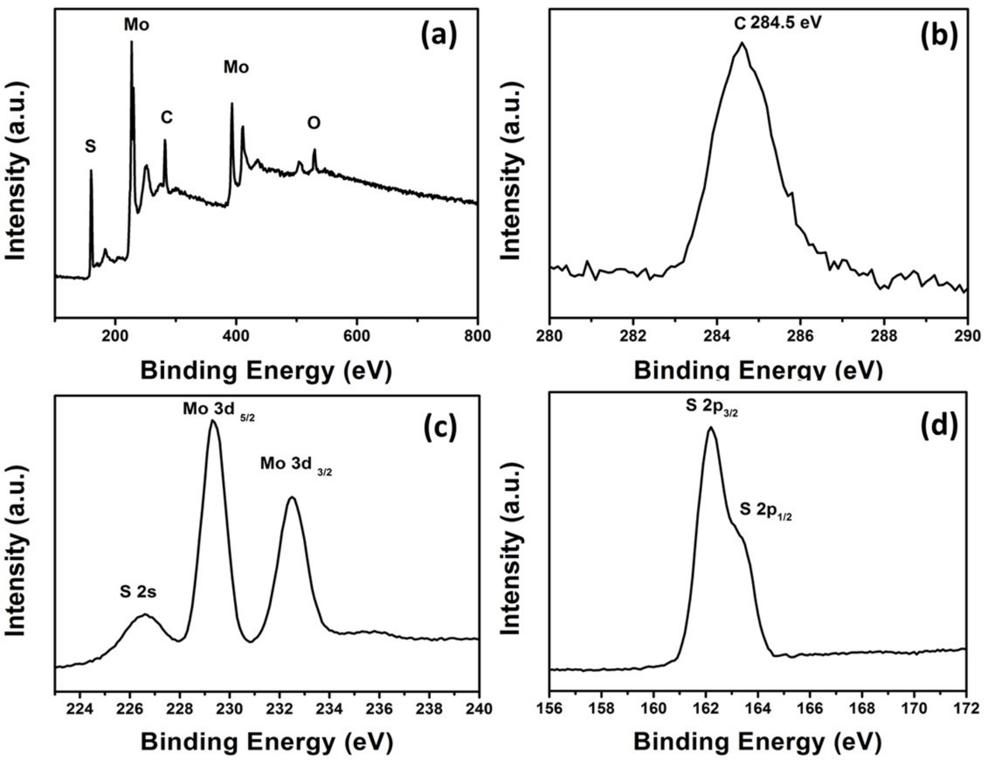

Figure S11 (a) XPS survey spectrum and high-resolution scans for the (b) C 1s, (c) Mo 3d and (d) S 2p electrons of ML-MoS_2.

The XPS of Mo 3d spectra and S 2p spectra of ML-MoS_2 sample was shown in Figure S11. The XPS spectra in the Mo 3d region (Figure S11c) exhibit four characteristic peaks which can be attributed to $3d_{3/2}$ at 232.6 eV, $3d_{5/2}$ at 229.4 eV for Mo (+4). The small peak (Mo 3d region) at 226.6 eV represents S 2s bonded to Mo. S 2p (Figure S11d) displayed S $2p_{3/2}$ peak at 162.1 and S $2p_{1/2}$ peak 163.3 eV.

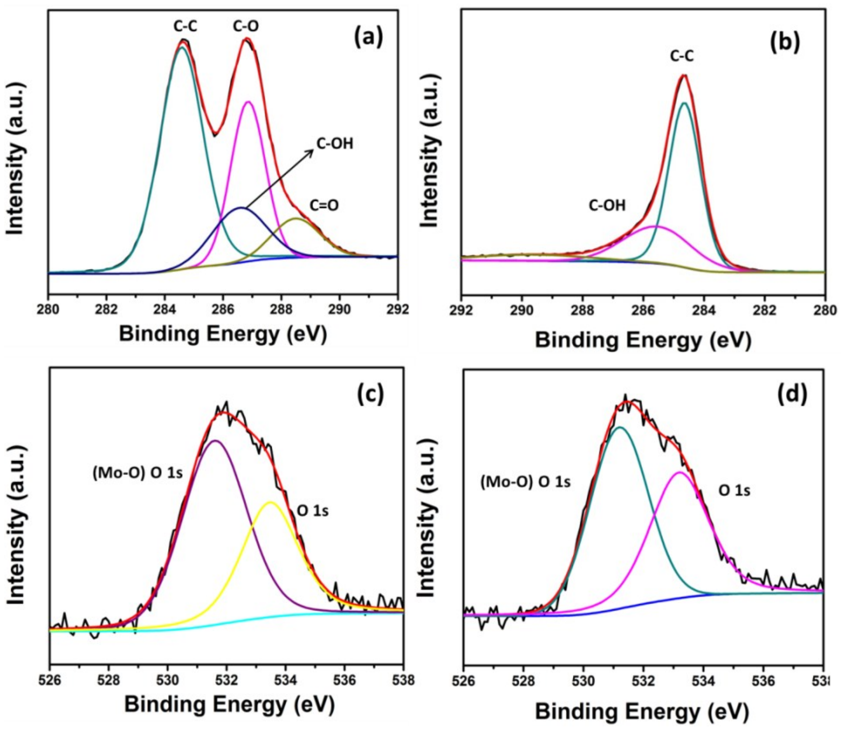

Figure S12 XPS of C1s spectra of (a) GONRs and (b) GNRs, O1s spectra of SL-MoS_2/GNRs and (b) FL-MoS_2/GNRs.

After the oxidation process, C–O (epoxy or alkoxy) and C=O (carbonyl or carboxyl) groups appear, which are located at 286.7 eV and 288.5 eV, respectively, in the C1s spectra of GONRs shown in Figure S12a. Some oxygen-containing functional groups such as C-OH have been remained in GNRs after annealing at 700 ^{o}C (shown in Figure S12b). In addition, the O 1s peak (shown in Figure S12c-d) located at 530.4 eV, corresponding to the binding energy of the oxygen incorporated into the MoS_2 ultrathin nanoplate lattice, indicates the existence of Mo–O bonds; this may result from the oxidation of unsaturated Mo by oxygen[8], also leading to the formation of Mo^{5+}. On the other hand, O atoms grafted on the MoS_2 ultrathin nanosheets via Mo^{5+}–O bonds, leading to the breaking of Mo–S–Mo bonds and production of defect sites, which leads to basal plane disorder in the local structure and expands interlayer spacing[9].

Table S1 Active sites of various catalysts and kinetic parameters of the reaction over the catalysts.

Cat.	T (^{o}C)	$(k\times10^{-6})^{a}$ (mol·s^{-1}·g$_{cat}$$^{-1}$)	Active sites^{b} (μmol·g$_{cat}$$^{-1}$)	TOF^{c} (s^{-1})	E_a^{a} (kJ·mol^{-1})
SL-MoS$_2$/GNRs	200	0.13	10.1		81.6
	220	0.30			
	240	0.67		0.07	
FL-MoS$_2$/GNRs	240	0.08	4.1	0.02	111.9
	260	0.21			
	280	0.55			
ML-MoS$_2$	240	0.01	1.2	0.01	112.9
	260	0.02			
	280	0.06			

[a] Measured from differential reaction of 500 ppm COS + N_2.

[b] The data detected by CO pulse adsorption at room temperature.

[c] Calculated based on the data detected by differential reaction and CO pulse adsorption..

The active sites were measured by CO pulse adsorption (Autochem II 2920, Micromeritics, USA). Each sample (50 mg) was pretreated at 500 ^{o}C for 60 min in He flow. Then it was subsequently cooled down to RT, 5% CO/He was injected in pulses until saturated adsorption was reached. The chemisorption of NO, O_2 or CO has been frequently and widely used to evaluate the dispersion of active phase in HDS catalyst[10, 11]. In the present work, CO pulse adsorption was used to calculate the active sites on the catalyst surface. They were 10.1 μmol·g^{-1} for SL-MoS$_2$/GNRs, 4.1 μmol·g^{-1} for FL-MoS$_2$/GNRs, and 1.2 μmol·g^{-1} for ML-MoS$_2$. On this basis, TOF value of the reaction over different catalyst was calculated and summarized in Table 1, which indicates that the HDS reaction at 240 ^{o}C occurs with 0.07, 0.02 and 0.01 s^{-1} over SL-MoS$_2$/GNRs, FL-MoS$_2$/GNRs and ML-MoS$_2$, respectively. Clearly, the TOF of SL-MoS$_2$/GNRs was 3.5 times that of FL-MoS$_2$/GNRs and 7 times that of bulk ML-MoS$_2$.

References

1. S. Park, J. An, J. R. Potts, A. Velamakanni, S. Murali and R. S. Ruoff, *Carbon*, 2011, **49**, 3019-3023.
2. W. Lai, Z. Chen, J. Zhu, L. Yang, J. Zheng, X. Yi and W. Fang, *Nanoscale*, 2016, **8**, 3823-3833.
3. O. Y. Gutierrez and T. Klimova, *J Catal*, 2011, **281**, 50-62.
4. G. C. Huang, T. Chen, W. X. Chen, Z. Wang, K. Chang, L. Ma, F. H. Huang, D. Y. Chen and J. Y. Lee, *Small*, 2013, **9**, 3693-3703.
5. C. F. Zhang, Z. Y. Wang, Z. P. Guo and X. W. Lou, *ACS Appl Mater Inter*, 2012, **4**, 3765-3768.
6. S. J. Ding, J. S. Chen and X. W. Lou, *Chem-Eur J*, 2011, **17**, 13142-13145.
7. G. X. Wang, J. Yang, J. Park, X. L. Gou, B. Wang, H. Liu and J. Yao, *J Phys Chem C*, 2008, **112**, 8192-8195.
8. J. F. Xie, J. J. Zhang, S. Li, F. Grote, X. D. Zhang, H. Zhang, R. X. Wang, Y. Lei, B. C. Pan and Y. Xie, *J Am Chem Soc*, 2013, **135**, 17881-17888.
9. J. H. Xiong, Y. H. Liu, D. K. Wang, S. J. Liang, W. M. Wu and L. Wu, *J Mater Chem A*, 2015, **3**, 12631-12635.
10. R. Burch and A. Collins, *Appl Catal*, 1985, **17**, 273-308.
11. T. Kubota, K. Sato, A. Kato, Usman, T. Ebihara, T. Fujikawa, Y. Araki, K. Ishida and Y. Okamoto, *Appl Catal a-Gen*, 2005, **290**, 17-24.